A 3-Dimentional Multiscale Model to Simulate Tumor Progression in Response to Interactions between Cancer Stem Cells and Tumor Microenvironmental Factors

Hua Tan[1,2+], Fuhai Li[1+], Jaykrishna Singh[1], Xiaofeng Xia[1], Derek Cridebring[1], Jian Yang[1], Ming Zhan[1]*, and Stephen T.C. Wong[1]*

NCI Center for Modeling Cancer Development, Department of Systems Medicine and Bioengineering
The Methodist Hospital Research Institute, Weil Medical College of Cornell University
Houston, Tx, U.S.A.
+Authors contributed equally to this work
Corresponding authors: {mzhan, stwong}@tmhs.org

Jiguang Bao[2], Jinwen Ma[3]
[2]School of Mathematical Sciences, Beijing Normal University, Laboratory of Mathematics and Complex Systems, Ministry of Education, Beijing, China

[3]Department of Information Science, School of Mathematical Sciences & LMAM, Peking University, Beijing, China

Abstract—**The recent discovery of cancer stem cells (CSCs), or tumor initiating cells (TICs), in a variety of cancers, including breast cancer, provides a key to understand the processes of tumor initiation, progression and recurrence. Here, we present a three-dimensional (3D) multiscale model of the CSC-initiated tumor growth, which takes into account essential microenvironmental (mE) factors (e.g. nutrients, extracellular matrix) and some important biological traits (e.g. angiogenesis, cell apoptosis, and necrosis) and addresses tumor growth from three different levels, i.e. molecular, cellular and tissue levels. At the molecular level, mathematical diffusion-reaction equations are used to understand the dynamics of mE factors. At the cellular level, a cellular automaton is designed to simulate the life cycle and behaviors of individual cells. At the tissue level, a computer graphics method is used to illustrate the geometry of the whole tumor. The simulation study based on the proposed model indicates that the content of CSCs in a tumor mass plays an essential role in driving tumor growth. The simulation also highlights the significance of developing therapeutic agents that can deliver drug molecules into the interior of the tumor, where most of CSCs tend to reside. The simulation study on the breast cancer xenografts reveals that the mouse tumor initiated from a mixed population of human CSCs and other tumor cells show a faster growth rate, while a weaker proliferation and aggressiveness than that initiated from a pure human CSCs population. These simulation results are mostly consistent with our experimental observations. The mathematical model thus provides a new framework for the modeling and simulation studies of CSC-initiated cancer development.**

Keywords—**cancer stem cells; multiscale modeling; tumor development;drug treatment.**

I. INTRODUCTION

Tumor is a complex disease, and the processes that drive tumor progression, e.g. angiogenesis, tissue invasion, metastasis and resistance to drug treatment remain unclear. Recently, experimental and clinical studies have reported that tumor progression depends on the existence of a small subset of cells called cancer stem cells (CSCs) or tumor initiating cells (TICs) [1-5]. The CSCs have extensive self-renewal potential, and are able to re-grow into a tumor through asymmetric proliferation [2, 6]. It is hypothesized that CSCs are the root that cause for therapeutic failures and tumor recurrence [3, 7]. Though the CSC concept offers reformative insights into tumor development and treatment, the roles of CSCs in tumor development and treatment remain unclear because even a tiny piece tissue of a tumor is a complex system, including signaling transduction inside and outside of cells, and thus it is technically difficult to investigate individual CSCs in such a complex system.

Mathematical models enable us to simulate, predict and validate the non-intuitive and complex hypotheses of tumor development [8-13]. In general, three groups of models have been widely used for the tumor development simulation, i.e. cellular (discrete), continuum, and hybrid models (integration of cellular and continuum models). In the cellular model (e.g. cellular automaton [14] and cellular potts models [15]), cancer cells are simulated individually, and cell behaviors are governed by a set of deterministic or probabilistic rules. In the continuum model, cancer-related variables such as cell population, nutrient and drug concentrations and concentration of other mE factors are modeled using a set of ordinary or partial differential equations [11, 16]. In the hybrid approach, nutrient concentrations, drug concentrations, and other mE

factors are modeled as continuous variables and cancer cells are modeled as discrete variables, and the behaviors of individual cancer cells are subject to the spatial dynamics of mE factors [8]. A few mathematical models have been proposed to investigate the roles of CSCs in tumor progression, [9, 10, 12, 13]. However, the effects of mE factors to CSCs and roles of CSCs, progenitor cells (PCs) and differentiated tumor cells (TCs) as well as the effects of CSC content, have not been fully investigated through 3D modeling.

Herein we propose a 3D and multiscale computational model to simulate tumor progression in response to interactions between CSCs and tumor mE factors. Fig. 1 shows mE factors and their effects on tumor cell behaviors that are described by the model. As indicated, when a small avascular tumor grows beyond its critical size, the cells in the interior of the tumor begin to die or be quiescent because of hypoxia. The dying cells then release tumor angiogenesis factors (TAFs), which diffuse into the surrounding tissues and activate endothelial cells (EC) to form neovasculature toward the hypoxia regions [18]. The tumor cells, on the other hand, may secrete the matrix degrading proteolytic enzyme (MDE) (e.g. fibronectin) to dilute the extracellular matrix (ECM) to create space for their migration [19].
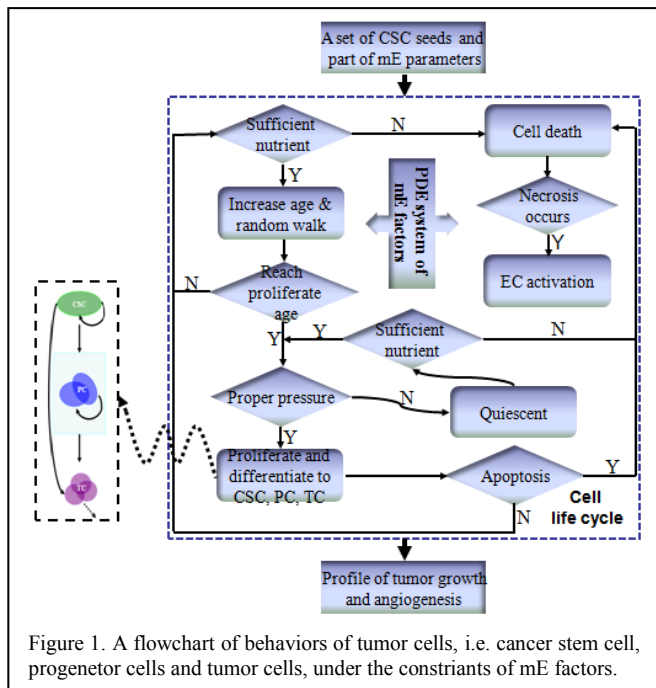

Figure 1. A flowchart of behaviors of tumor cells, i.e. cancer stem cell, progenetor cells and tumor cells, under the constraints of mE factors.

The proposed model is designed in the 3D space and multi-scale, consisting of three biological scales: molecular, cellular, and tissue, as shown in Fig. 2. At the molecular level, the adaptive finite element method is employed to solve the PDE system that describes the diffusion and reactions of mE factors, i.e. nutrients, TAF, MDE, ECM and tissue pressure (also known as interstitial fluid pressure [20]). At the cellular level, a 3D cellular automaton is designed to describe the cell behaviors. We allow a hierarchical organization of tumor cell

subtypes, including CSC, PC and TC, as shown in Fig. 1. At the tissue level, the global visualization of tumor is presented.

Based on the proposed model, we conducted simulations on CSC-initiated tumor development. The results indicated that the content of CSCs in a tumor plays an essential role in tumor growth. The results also suggest that it is critical to develop therapeutic agents that can penetrate and deliver drug molecules into the interior of tumor, where most CSCs are located. By simulating the development of xenografted tumor
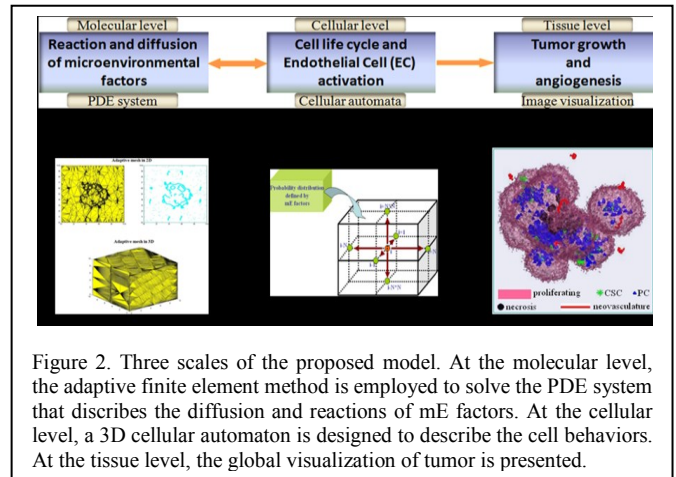

Figure 2. Three scales of the proposed model. At the molecular level, the adaptive finite element method is employed to solve the PDE system that discribes the diffusion and reactions of mE factors. At the cellular level, a 3D cellular automaton is designed to describe the cell behaviors. At the tissue level, the global visualization of tumor is presented.

in mice, we observed a faster growth rate while a weaker proliferation and aggressiveness in the tumor initiated from a mixed population of human CSCs and other tumor cells than the tumor initiated from a pure human CSC population. These simulation results are consistent with our experimental observations. The proposed model and simulation thus provide us a new computational framework for exploration of CSC-initiated cancer development.

II. MATERIALS AND METHODS

A. Animal and Tumor Samples

Breast cancer tissues were obtained from patients undergoing surgical resection after informed consent. Two groups of NOD/SCID mice were prepared for flank injection. One group (n = 5) was injected with 1×10^3 breast cancer cells, which are all CSCs identified as CD44+/CD24-. Another group (n = 4) was injected with 1×10^6 breast cancer cells in which 4.1% are CSCS (CD44+/CD24-). The CD44+/CD24- are general biomarkers for identifying breast CSCs [21]. All nine of the injections formed tumors, and the diameter of each tumor was measured every other day until they reached about 2 cm in size, which is a constraint imposed by our Institutional Animal Care and Use Committee (IACUC).

B. The PDE System Describing mE Factors

The following is the system of PDEs describing the diffusion and reactions of five mE factors, including nutrients (*n*), TAF (*c*), MDE (*m*), fibronectin (*f*), and tissue pressure (*p*). For simplification, domain symbol Ω is omitted in each equation, except where noted. All variables and parameters

involved are non-dimensional. Also an indicator function χ_Ω defined in a domain Ω is defined as: $\chi_\Omega(x) = 1$, if $x \in \Omega$; $\chi_\Omega(x) = 0$, if $x \notin \Omega$.

The diffusion-reaction profile of nutrients is depicted by the following quasi-steady equation with non-zero Dirichlet boundary conditions [22, 23].

$$
\begin{cases}
0 = \overbrace{D_n \nabla^2 n} - \lambda_u^n n \\
\quad + \overbrace{\chi_{(\Omega_V \cup \Omega_H)}(1-n)(K_{pa}^n(p)\chi_{\Sigma_C} + \lambda_{pp}^n) + \lambda_b^n f} \\
n|_{\partial\Omega} = 1, \qquad K_{pa}^n(p) = \lambda_{pa}^n(1-p)
\end{cases}
\tag{1}
$$

where D_n is the nutrient diffusion coefficient, and λ_{pp}^n and λ_{pa}^n are rates of nutrient transfer from preexisting and neo-vasculature blood vessels, respectively. λ_b^n is the rate of binding to fibronectin, and λ_u^n is the rate of uptake by all cells, which varies with different cell types. χ_{Σ_c} is the indicator function of the neo-vasculature. By multiplying the pressure term $(1-p)$, the heterogeneity of the blood vessels was implicitly incorporated in terms of nutrient transfer, where p is the hydrostatic/oncotic pressure. Further, the term $(1-p)$ was incorporated in K_{pa}^n to adapt the saturation effect of nutrient transfer; more specifically, the transfer was depressed with increase to the pressure outside the vessels [22, 23].

The TAF released by the tumor cells, especially dying tumor cells, diffuses throughout the tumor region. During diffusion, it may be ingested by endothelial cells or degrade naturally. This process is modeled by the following Neumann problem [22, 23]:

$$
\begin{cases}
0 = \overbrace{D_c \nabla^2 c} + \overbrace{\lambda_{pN}^c \chi_{\partial\Omega_N} + \lambda_{pV}^c \chi_{\Omega_V}} - \overbrace{\lambda_u^c c \chi_{\Sigma_C}} - \lambda_d^c c \\
\dfrac{\partial}{\partial \vec{n}}
\end{cases}
\tag{2}
$$

where D_c is the TAF diffusion coefficient, $\partial\Omega_N$ is the necrotic-viable interface, $\vec{n}$ is the unit outer normal direction on the boundary of Ω, λ_{pN}^c and λ_{pV}^c are rates of secretion of TAF by dying cells and by viable cells, respectively, λ_u^c is the rate of uptake by endothelial cells, and λ_d^c is the rate of degradation.

Fibronectin is one of major components of ECM, which is a long binding molecule that does not diffuse but does enhance cell adhesion to the extracellular matrix of the surrounding tissue. The concentration of fibronectin obeys:

$$
\begin{cases}
\dfrac{\partial f}{\partial t} = \overbrace{\lambda_p^f(1-f)\chi_{\Omega_V} + \lambda_{sp}^f \chi_{\Sigma_C}} - \overbrace{\lambda_d^f fm}^{\text{radation}} \\
f|_{t=0} = 1
\end{cases}
\tag{3}
$$

where λ_p^f and λ_{sp}^f are rates of production of fibronectin by the viable tumor cells and endothelial cells constituting the neovasculature, respectively, and λ_d^f stands for the rate of degradation of ECM by the MDE.

The MDE secreted by both viable tumor cells and endothelial cells causes the degradation of the ECM, subsequently providing space for cells. The diffusion, production and degradation of MDE are described as:

$$
\begin{cases}
0 = \overbrace{D_m \nabla^2 m} + \overbrace{\lambda_p^m(1-m)\chi_{\Omega_V} + \lambda_{sp}^m \chi_{\Sigma_C}} - \lambda_d^m m^{\text{cay}} \\
\dfrac{\partial m}{\partial \vec{n}}
\end{cases}
\tag{4}
$$

where, D_m is the diffusion coefficient while the other three parameters correspond to those in (3).

Cell velocity is related to tissue pressure, which results from heterogeneous cell proliferation presented by the following equation, known as Darcy-Stokes (DS) law [22]: $\vec{u} = -\nabla p$, $p|_{\partial\Omega} = 0$. The velocity field of the cell motility obeys the following divergence equation:
$\nabla \cdot \vec{u} = \chi_{\Omega_V}(n - \lambda_a) - \chi_{\Omega_N}\lambda_N$, where, λ_a and λ_N are the rates of volume loss due to apoptosis and necrosis. Here, the first term on the left side is regarded as the source effect, and the second term is considered as the sink effect due to cell apoptosis. A divergence on both sides of the DS law equation is performed and combined with the divergence equation of cell motility to yield the diffusion equation of pressure:

$$
\begin{cases}
0 = \nabla^2 p + (n - \lambda_a)\chi_{\Omega_V} - \lambda_N \chi_{\Omega_N} \\
p|_{\partial\Omega} = 0
\end{cases}
\tag{5}
$$

The PDEs containing the diffusion items are solved by the finite element method with adaptive mesh as demonstrated in [24]. Cell velocity was calculated by equation (5) and the equation of ECM was solved by the 2nd order total variation Runge-Kutta method [25]. Finally, the time step Δt was calculated at each time point [22] for the sake of computational stability: $\Delta t = (\Delta l/4).\min\{1/\max_i|V_i|, 1/\max_i|\vec{u_i}|\}$, where $\Delta l = 0.1$ stands for the spatial step in all the simulations, V_i is a function of TAF, ECM, and cell velocity at each spatial point i [22], and $\vec{u_i}$ represents cell velocity at spatial point i.

C. 3D Cellular Automaton

Each cell could migrate or generate a new cell into one of its six orthogonal neighbors, considering the status of mE

factors at each time step. In specific, for a given cell located at grid k:

1) Check all the empty immediate orthogonal neighbor grids that are not occupied by cells.

2) If there is no empty neighbor grid, then go to 8).

3) The cell migration probabilities to the m ($m<=6$) immediate orthogonal neighbors are calculated as: $q_i=n_i/f_i$, $i=0,1,2,...,m$, where q_0 denotes the probability of staying at the same grid.

4) Let $q_k^{'}=\sum_{i=1}^{k}q_i$, then we get a monotonically increasing vector: $[q_0^{'},q_1^{'},...,q_m^{'}]$, and normalize them as: $q_i^{''}=q_i^{'}/q_m^{'}$.

6) Define $R_1=[0,q_1^{''}]$, and $R_i=[q_{i-1}^{''},q_i^{''}]$, $i = 1,2,...,m$.

7) Generate a random number r uniformly from [0, 1], check which interval does r belong to, and then migrate the cell to the grid corresponding to the selected interval.

8) Increase the age of the cell. Check whether the cell would divide or not. If it divides, increase one cell with a proper cell type, and let it migrate following the above migration rules. Check whether the cell would become quiescent or death due to mE conditions, e.g. nutrients and drugs.

D. Gompertz Curve Fitting and Metrics

The Gompertz curve describes a growth pattern which is slow in both the beginning and the end, but is fast in between, and has been considered to be a good mathematical descriptor of untreated tumor growth [26]. It is defined as: $y(t) = y_0 \exp(k(1-\mathrm{e}^{-b(t-t_0)}))$, where y_0 is the tumor volume at time t_0, while k and b (both positive) are parameters relating to the axis displacement and growth rate. The four parameters are estimated as: $(\bar{k},\bar{b},\bar{y}_0,\bar{t}_0)=\underset{(k,b,y_0,t_0)}{\arg\min}\sum_{i=1}^{N}(y(t_i)-y_i)^2$, where y_i is the measured tumor volume at time t_i, and N is the number of observations. The properties of tumor are measured by four metrics: the Proliferation Potential (*PP*), the Time a tumor needs to reach its Potential (*TtP*), the Average Aggressive Index (*AAI*) and the Average Fitting Error (*AFE*) when fitted to the Gompertz curve. Specifically, *PP* was calculated as: $PP = \lim_{t\to\infty} y(t) = y_0 e^k$. It is used to estimate the potential size of a tumor. *TtP* was obtained as: $TtP = \inf\{t>0; y(t) \ge PP\}$, 'inf' means the infimum of a set. The aggressiveness metric, *AAI*, is defined as: $AAI = \frac{1}{N}\sum_{i=1}^{N}\frac{S_i}{V_i}$, where S_i and V_i denote the surface and volume of the tumor i. The metric *AFE* is defined as: $AFE = \sqrt{\sum_{i=1}^{N}(y(t_i)-y_i)^2/N}$.

III. RESULTS

A. Determination of parameters important to tumor growth

Table 1 lists the parameters of the proposed model. The continuous parameters are related to the PDE system, and the discrete parameters are used in the cellular automaton. The values of the parameters were determiend from literatures or estimated from experimental data.

To determine which parameters of the model contributed significantly to the final equilibrium state (or stable steady state) of tumor growth, we performed sensitivity analysis. The final tumor volume was estimated by perturbing the parameter values in a range of 10%. In each simulation, the total number of tumor cells (CSCs + PCs + TCs) was calculated after the model reached a steady state. Specifically, we observed a few parameters' values are relative sensitive to the tumor growth, including some continuous parameters, i.e., λ_{pp}^n (the rate of nutrient transfer from pre-existing blood vessels), λ_{pN}^c (the rate of secretion of TAF by dying cells), λ_p^m (the rate of production of MDE by viable tumor cells), D_c (the TAF diffusion coefficient); and some important symmetric and asymmetric proliferation abilities of tumor cells, i.e., K_{CCP} (the probability that CSC divide asymmetrically to generate one CSC and one PC) and K_{PP} (the probability that PCs divide symmetrically to two progenitor cells).

TABLE I.   SUMMARY OF ALL THE CONTINUOUS AND DISCRETE PARAMETERS USED IN THE MULTISCALE CSC MODEL.

Symbol	Description	Value	Source
Continuous Parameters			
D_n	Nutrient diffusion coefficient	1.0	PM2009
D_c	TAF diffusion coefficient	100	Estimated
D_m	MDE diffusion coefficient	1.0	PM2009
λ_u^n	Rate of nutrient uptake	[0.2,0.5,0.33, 0.67, 1, 1]	XZ2005; Estimated
λ_b^n	Rate of binding of nutrient	2.5·e-3	Estimated
λ_{pa}^n	Rate of nutrient transfer from neovasculature	0.05	XZ2005; Estimated
λ_{pp}^n	Rate of nutrient transfer from existing vessel	0.01	Estimated
λ_{pN}^c	Rate of production of TAF by dying cells	0.05	Estimated
λ_{pV}^c	Rate of production of TAF by viable cells	0.004	Estimated
λ_d^c	Rate of degradation of TAF	0.01	PM2009
λ_u^c	Rate of uptake of TAF by endothelial cells	0.025	PM2009
λ_p^m	Rate of production of MDE by viable cells	{50,100,150 }	PM2009; Estimated
λ_{sp}^m	Rate of production of MDE by endothelial cells	1.0	PM2009
λ_d^m	Rate of degradation of MDE	10	PM2009

λ_p^f	Rate of production of ECM by viable cells	0.1	PM2009
λ_{sp}^f	Rate of production of ECM by endothelial cells	0.01	Estimated
λ_d^f	Rate of dissolution of ECM	0.01	PM2009
λ_a	Rate of volume loss due to apoptosis	0~0.00013	Estimated
λ_N	Rate of volume loss due to necrosis	0.25	XZ2005
θ_a	Minimum nutrient concentration for cell survival	{0.1, 0.17, 0.25}	XZ2005; Estimated
θ_d	Maximum drug concentration for cell survival	{0.25, 0.27, 0.375}	Estimated
Discrete Parameters			
$[K_{CC}, K_{CCP}, K_{CP}, K_{CT}]$	Probabilities related to CSC proliferation	{0.6,0.25,0.1, 0.05}	Estimated
$[K_{PP}, K_{PT}]$	Probabilities related to PC proliferation	{0.25,0.75}	Estimated
$[K_{TT}, d_T]$	Probabilities related to TC proliferation	$[1-\lambda_a, \lambda_a]$	Estimated
A_p	Proliferation ages of cells	$\delta_t \cdot [5, 2, 5, 1]$	Estimated
G_m	Maximum generations a cell can proliferate	$\delta_m \cdot [10, 2, 1]$	Estimated
C_s	Constant for cell size scaling	$10 \cdot e\text{-}5$	Estimated

B. Simulation of CSC-Initiated Tumor Development

We simulated the breast cancer tumor development under two experimental conditions of CSC initiation. We then validated the simulated results by the corresponding experiment data so that justified the proposed mathematical model. The two experiments, i.e. the breast cancer xenografting with sorted and unsorted human CSC cells, are
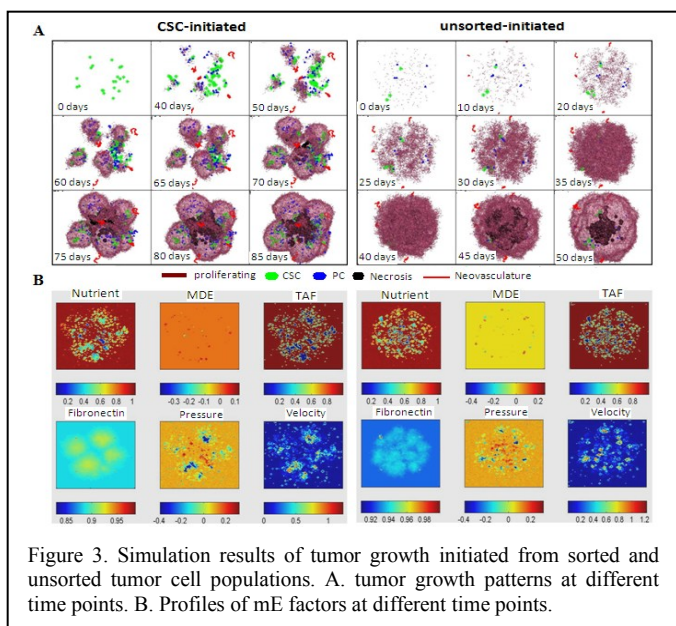

Figure 3. Simulation results of tumor growth initiated from sorted and unsorted tumor cell populations. A. tumor growth patterns at different time points. B. Profiles of mE factors at different time points.

described in the method part. In the simulation corresponding to the sorted experiment, tumor growth in mouse was initiated by a set of pure CSCs population (~20 CSCs). In the simulation corresponding to the unsorted experiment, tumor growth in mouse was initiated by a mixed population of CSCs

and niche cells (~500 cells with 4% cells as CSCs). Fig. 3 shows the tumor growth and mE factor profiles in the two simulations. Tumors initiated from the unsorted cells grow to the limit size much faster (~50 days) than that from the sorted cells (~85 days). Interestingly, the tumor derived from the sorted CSCs has fingered irregular morphology, in comparison with the tumor from unsorted cells. The fingered morphology is probably caused by the individual CSCs generated their own colonies. These simulated results are consistent to our experimental observations.

To further investigate how CSCs affect tumor growth, we conducted simulations, in which the initial proportion of CSCs was set to be 4%, 50%, and 100%, respectively, with the initial number of cancer cells fixed (50 tumor cells). Fig. 4 shows the four metrics of simulation results. As shown, proliferation potential and aggressiveness of tumors significantly increases with the increase of CSC fraction, and the time needed to reach the proliferation potential (*TtP*) also generally increases as the CSCs' fraction increases. However, the tumors initiated from the pure population of CSCs reach their limit size slightly faster than the ones initiated from 50% CSCs. This is because CSCs may proliferate fast under certain mE factors such as nutrient and ECM concentrations during the tumor growth. We also found that the tumor derived from the pure CSCs have a smaller average fitting error, which indicates that the growth of the pure CSCs more resembles the Gompertz curve that mixed tumor cells (CSCs+non-CSCs). In conclusion, the content of CSCs in a tumor mass plays an essential role in driving tumor growth, which is consistent with our experimental observations.
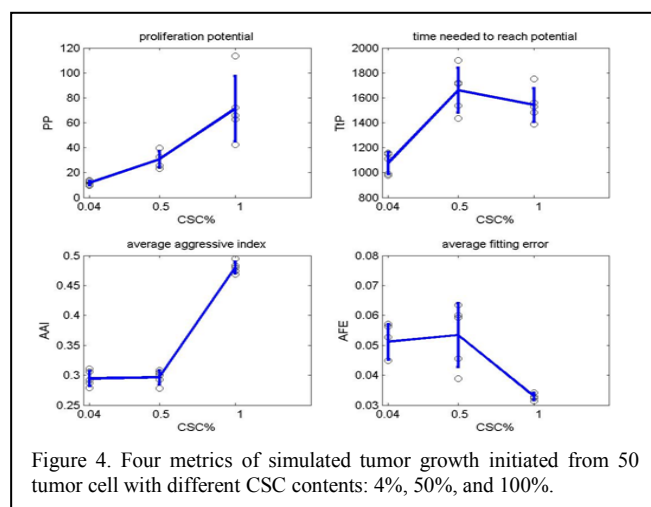

Figure 4. Four metrics of simulated tumor growth initiated from 50 tumor cell with different CSC contents: 4%, 50%, and 100%.

C. Simulation of tumor response to drug treatment

We also conducted a simulation of chemotherapy on tumor growth. We assumed that both cancer cells and CSCs could be killed when the drug concentration reaches a threshold level, and we set different threshold values for CSCs and tumor cells. Fig. 5 shows the simulated dynamics of drug treatment. As illustrated, during the drug treatment the solid tumor shrinks while the fraction of CSCs increases, which is consistent with experimental observations and clinical reports [27]. It is also shown that once the treatment stops, the solid tumor grows to a half of its original size within a short period of time. The percentage of CSCs in the re-grown tumors is significantly larger than that before treatment. The fast re-growth and increased fraction of CSCs during tumor re-growth are indicative of the aggressiveness of the relapsed tumors. The fast relapse is probably because that the drug treatment first induced the death of most non-CSCs, residing in the rim of tumors, and consequently, once the drug treatment is stopped, more space and nutrient would be available for CSCs that tend to reside in the interior of tumors.
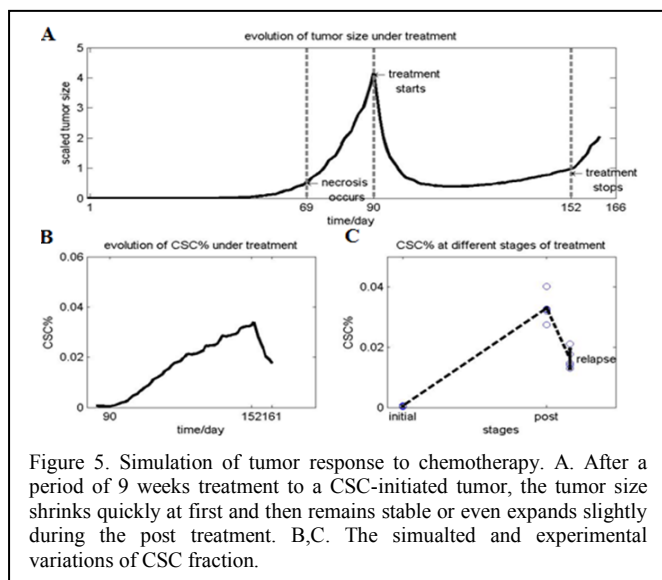

Figure 5. Simulation of tumor response to chemotherapy. A. After a period of 9 weeks treatment to a CSC-initiated tumor, the tumor size shrinks quickly at first and then remains stable or even expands slightly during the post treatment. B,C. The simualted and experimental variations of CSC fraction.

IV. DISCUSSION

In this study, a 3D and multiscale model of tumor growth is developed to investigate how CSCs interact with mE factors to drive tumor progression. Multiple important mE factors and biological processes important to tumor development are incorporated into the model. The model is implemented on a 3D platform at three hierarchical levels (e.g. molecular, cellular and tissue levels). The proposed computational model could be easily modified and extended to different applications in CSC-related studies.

The proposed model predicts important insights into caner development and drug treatment. Through the modeling, we found, for example, that the neovasculature can extend into the interior of a tumor during its evolution. This implies that the neovasculature might help deliver drugs into the interior of

a tumor, where CSCs reside. We also found that the mouse tumor initiated by the sorted human CSC population have enhanced proliferation potential and stronger aggressiveness, while the growth of tumors from the unsorted cells is faster than that from the sorted cells. The mathematical simulations also explain the aggressive recurrence of tumors once medication is stopped. These findings may motivate the implementation of localized drug delivery that can deliver drug into the interior of a tumor and target at the CSC subpopulation effectively.

Our current model treats the metabolism of a tumor in a simple manner. We allow the nutrients to diffuse among the tumor region according to dynamic principles and clear the apoptotic or killed cells forcefully. These processes, however, involve complex biochemical reactions. Relevant regulatory or signaling pathways, particularly those related to proliferation of cancer cells need to be considered. Moreover, different drugs might target on different cell populations. Specific effects of drugs should be considered to accurately simulate their effects. Last but not the least, the cell shape impacts cell-cell and cell-mE factor interactions, particularly when the cell density is dense, causing shape deformation and cell-cell interaction through cell surface markers. We will thus take this as well as others into account as part of our further improvements of the proposed model.

REFERENCES

1   Reya, T., Morrison, S.J., Clarke, M.F., and Weissman, I.L.: 'Stem cells, cancer, and cancer stem cells', Nature, 2001, 414, (6859), pp. 105-111

2   Pardal, R., Clarke, M.F., and Morrison, S.J.: 'Applying the principles of stem-cell biology to cancer', Nat Rev Cancer, 2003, 3, (12), pp. 895-902

3   Rich, J.N.: 'Cancer stem cells in radiation resistance', Cancer Res, 2007, 67, (19), pp. 8980-8984

4   Zhang, M., Behbod, F., Atkinson, R.L., Landis, M.D., Kittrell, F., Edwards, D., Medina, D., Tsimelzon, A., Hilsenbeck, S., Green, J.E., Michalowska, A.M., and Rosen, J.M.: 'Identification of tumor-initiating cells in a p53-null mouse model of breast cancer', Cancer Res, 2008, 68, (12), pp. 4674-4682

5   Malanchi, I., Santamaria-Martinez, A., Susanto, E., Peng, H., Lehr, H.-A., Delaloye, J.-F., and Huelsken, J.: 'Interactions between cancer stem cells and their niche govern metastatic colonization', Nature, 2011, 481, (7379), pp. 85-89

6   Huntly, B.J., and Gilliland, D.G.: 'Cancer biology: summing up cancer stem cells', Nature, 2005, 435, (7046), pp. 1169-1170

7   Zhang, M., Atkinson, R.L., and Rosen, J.M.: 'Selective targeting of radiation-resistant tumor-initiating cells', Proc Natl Acad Sci U S A, 2010, 107, (8), pp. 3522-3527

8   Anderson, A.R.: 'A hybrid mathematical model of solid tumour invasion: the importance of cell adhesion', Math Med Biol, 2005, 22, (2), pp. 163-186

9 Ganguly, R., and Puri, I.K.: 'Mathematical model for the cancer stem cell hypothesis', Cell Prolif, 2006, 39, (1), pp. 3-14

10 Michor, F.: 'Mathematical models of cancer stem cells', J Clin Oncol, 2008, 26, (17), pp. 2854-2861

11 Frieboes, H.B., Zheng, X., Sun, C.H., Tromberg, B., Gatenby, R., and Cristini, V.: 'An integrated computational/experimental model of tumor invasion', Cancer Res, 2006, 66, (3), pp. 1597-1604

12 Sottoriva, A., Verhoeff, J.J.C., Borovski, T., McWeeney, S.K., Naumov, L., Medema, J.P., Sloot, P.M.A., and Vermeulen, L.: 'Cancer Stem Cell Tumor Model Reveals Invasive Morphology and Increased Phenotypical Heterogeneity', Cancer Research, 2010, 70, (1), pp. 46-56

13 Zhu, X., Zhou, X., Lewis, M.T., Xia, L., and Wong, S.: 'Cancer stem cell, niche and EGFR decide tumor development and treatment response: A bio-computational simulation study', J Theor Biol, 2011, 269, (1), pp. 138-149

14 Kansal, A.R., Torquato, S., Harsh, G.I., Chiocca, E.A., and Deisboeck, T.S.: 'Simulated brain tumor growth dynamics using a three-dimensional cellular automaton', J Theor Biol, 2000, 203, (4), pp. 367-382

15 Bauer, A.L., Jackson, T.L., and Jiang, Y.: 'A cell-based model exhibiting branching and anastomosis during tumor-induced angiogenesis', Biophys J, 2007, 92, (9), pp. 3105-3121

16 Frieboes, H.B., Lowengrub, J.S., Wise, S., Zheng, X., Macklin, P., Bearer, E.L., and Cristini, V.: 'Computer simulation of glioma growth and morphology', Neuroimage, 2007, 37 Suppl 1, pp. S59-70

17 Shimizu, S., Eguchi, Y., Kamiike, W., Itoh, Y., Hasegawa, J.-i., Yamabe, K., Otsuki, Y., Matsuda, H., and Tsujimoto, Y.: 'Induction of Apoptosis as well as Necrosis by Hypoxia and Predominant Prevention of Apoptosis by Bcl-2 and Bcl-XL', Cancer Research, 1996, 56, (9), pp. 2161-2166

18 Ferrara, N.: 'VEGF and the quest for tumour angiogenesis factors', Nat Rev Cancer, 2002, 2, (10), pp. 795-803

19 Stetler-Stevenson, W.G., Aznavoorian, S., and Liotta, L.A.: 'Tumor Cell Interactions with the Extracellular Matrix During Invasion and Metastasis', Annual Review of Cell Biology, 1993, 9, (1), pp. 541-573

20 Hori, K., Suzuki, M., Abe, I., and Saito, S.: 'Increased tumor tissue pressure in association with the growth of rat tumors', Jpn J Cancer Res, 1986, 77, (1), pp. 65-73

21 Sheridan, C., Kishimoto, H., Fuchs, R., Mehrotra, S., Bhat-Nakshatri, P., Turner, C., Goulet, R., Badve, S., and Nakshatri, H.: 'CD44+/CD24- breast cancer cells exhibit enhanced invasive properties: an early step necessary for metastasis', Breast Cancer Research, 2006, 8, (5), pp. R59

22 Zheng, X., Wise, S.M., and Cristini, V.: 'Nonlinear simulation of tumor necrosis, neo-vascularization and tissue invasion via an adaptive finite-element/level-set method', Bull Math Biol, 2005, 67, (2), pp. 211-259

23 Macklin, P., McDougall, S., Anderson, A.R., Chaplain, M.A., Cristini, V., and Lowengrub, J.: 'Multiscale modelling and nonlinear simulation of vascular tumour growth', J Math Biol, 2009, 58, (4-5), pp. 765-798

24 Gockenbach, M.S.: 'Understanding and implementing the finite element method', Philadelphia: Society for Industrial and Applied Mathematics, 2006

25 Shu, S.G.a.C.: 'Total variation diminishing runge-kutta schemes', Mathematics of computation, 1998, 67, pp. 73-85

26 Norton, L.: 'A Gompertzian model of human breast cancer growth', Cancer Res, 1988, 48, (24 Pt 1), pp. 7067-7071

27 Li, X., Lewis, M.T., Huang, J., Gutierrez, C., Osborne, C.K., Wu, M.F., Hilsenbeck, S.G., Pavlick, A., Zhang, X., Chamness, G.C., Wong, H., Rosen, J., and Chang, J.C.: 'Intrinsic resistance of tumorigenic breast cancer cells to chemotherapy', J Natl Cancer Inst, 2008, 100, (9), pp. 672-679